Electronic Supplementary Material (ESI) for Journal of Materials Chemistry A.

Supplementary Information for

A robust cocatalyst Pd_4S uniformly anchored onto Bi_2S_3 nanorods for enhanced visible light photocatalysis

Lu-Lu Long,[†a] Ai-Yong Zhang,[†*ab] Yu-Xi Huang,[a] Xing Zhang,[a] Han-Qing Yu[*a]

[a] CAS Key Laboratory of Urban Pollutant Conversion, Department of Chemistry, University of Science & Technology of China, Hefei, 230026, China

[b] Department of Municipal Engineering, Hefei University of Technology, Hefei, 230009, China

Experimental Section

Reagents. Bismuth nitrate ($Bi(NO_3)_3$•$5H_2O$), palladium acetylacetonate ($Pd(acac)_2$), oleylamine, oleic acid were purchased from Aladdin (Aladdin Reagent Inc., China). Thioacetamide (C_2H_5NS), diphenyl oxide were purchased from Sinopharm Chemical Reagent (Sinopharm Co., China). All the chemicals were used as purchased without further purification, and deionized water (DI water) was used throughout the study. The polycrystalline TiO_2 P25 (Degussa Co, Germany) possesses a mean particle size of about 25 nm, anatase/rutile = 80:20 and a BET surface area of ca. 50 m^2/g.

Preparation of Bi_2S_3 Nanorods. Bi_2S_3 nanorods were synthesized through a simple hydrothermal procedure. In a typical reaction, 120 mg of $Bi(NO_3)_3 \cdot 5H_2O$ and 60 mg of C_2H_5NS were mixed with 20 mL of DI water. The mixed solution was treated by sonication for 5 min and then transferred into a Teflon-lined stainless steel autoclave, heated at 200 °C for 24 h, and then air-cooled to room temperature. The obtained black powders were centrifugated and washed thoroughly with DI water and dried at 50 °C for 12 h.

Preparation of Pd_4S/Bi_2S_3 Hybrid. The hybrid was synthesized using a facial method, in which Pd_4S nanoparticles were in-situ formed from Bi_2S_3 nanorods through a thermal reduction and subsequent cation-exchange. Briefly, 100 mg of the as-prepared Bi_2S_3 nanorods were dispersed in a solution containing 2 mL of oleylamine, 0.5 mL of oleic acid and 17 ml of diphenyl ether at 50 ^oC, and then 100 mg of $Pd(acac)_2$ was added. The mixture was stirred under nitrogen flush for 0.5 h, then heated to 200 ^oC and kept for 10 min. Afterwards, the flask was removed from heat and allowed to cool. The product was centrifuged by adding acetone. The obtained black powders were washed twice by precipitation and centrifugation in cyclohexane and ethanol. For comparison, the PdS/Bi_2S_3 hybrid was also prepared by prolonging the reaction time to 1 h at 200 ^oC, other conditions remained unchanged as for the Pd_4S/Bi_2S_3 hybrid.

Characterization. The Bi_2S_3 and Pd_4S/Bi_2S_3 catalysts were examined by X-ray diffraction (XRD) (Rigaku TTR-III, PHLIPS Co., the Netherlands) with Cu Kα radiation. X-ray photoelectron spectra (XPS) were recorded on an ESCALAB 250 instrument (VG Instrument Ltd., USA) with a monochromatic Mg Kα X-ray source to determine the chemical compositions and valence band. Transmission electron microscope (TEM) images were taken using a high-resolution TEM (JEM-2011, JEOL Co., Japan) with an acceleration voltage of 200 kV. High-resolution transmission electron microscope (HRTEM) images, selected-area electron diffraction (SAED), elemental mapping and energy-dispersive X-ray spectroscopy (EDS) were conducted on a JEM-ARM200F (JEOL Co., Japan). The diffuse reflectance spectra (DRS) were measured using a UV-Vis spectrophotometer (UV 2550, Shimadzu Co., Japan). The IR spectra were obtained using an infrared spectrometer (Vertex 70, Bruker Co., Germany). The ESR signal of the radicals spin-trapped by 5,5-dimethyl-

lpyrroline-N-oxide (DMPO) was recorded on a Bruker EPR A300 spectrometer. The irradiation source ($\lambda > 420$ nm) was a 300 W Xe arc lamp system, and the settings for the ESR spectrometer were as follows: center field = 3512 G, microwave frequency = 9.86 GHz, and power = 6.36 mW. Photoluminescence spectrum (PL) measurements were carried out by a fluorescence spectrophotometer (F-4600, Hitachi Co., Japan), containing a xenon lamp with 360 nm excitation wavelength at room temperature.

Electrochemical impedance spectroscopy (EIS) measurements were performed in 0.2 M Na_2S solution at open circuit potential over a frequency range from 105 to 10-1 Hz. Photocurrent data were obtained in 0.1 M Na_2SO_4 solution at 0.25 V (vs. KCl-saturated Ag/AgCl electrode). Mott-Schottky spectra measurement was performed in 0.3 M Na_2SO_4 solution at pH = 7.0. All the electrochemical tests were performed on a work station (CHI 660C, CH Instrument Co., China).

Photocatalytic Degradation of Atrazine. The photocatalytic activity of the as-prepared Pd_4S/Bi_2S_3 hybrid was evaluated by degrading atrazine (ATRZ, 10 mg L-1) under visible light irradiation. Typically, 3 mg of Pd_4S/Bi_2S_3 was dispersed in 30 mL mixed aqueous suspension containing 0.15 M of Na_2SO_3 and 0.1 M of Na_2S as sacrificial reagents. Prior to irradiation, the suspension was sonicated for 5 min and then magnetically stirred for 10 min to establish adsorption-desorption equilibrium. A 500 W Xenon lamp (wavelength > 420 nm by pass filter) was used as the visible light source. At given time intervals, an aliquot of the mixed solution was collected and centrifuged, and the residual ATRZ concentration in the supernatant was analyzed using high performance liquid chromatography (HPLC, 1100, Agilent Inc., USA) with a variable-wavelength detector (VWD) set at 220 nm. The mobile phase was consisted of H_2O and methanol (50:50), and the flow rate was 0.8 mL/min. The main degradation products of Atrazine on Pd_4S/Bi_2S_3 were identified by liquid chromatography-mass spectrometry (LC-MS, 6460, Agilent Inc., USA).

Results and Discussion

Formation of the Bi_2S_3 Nanorods. Fig. S1 shows the SEM images of the Bi_2S_3 nanostuctures at different reaction times: at 1 h, the obtained sample was dominantly composed of thin and short nanorods with a diameter of 100 nm and length of 500 nm (Fig. S1a); at 2 h, the thin and short nanorods started to connect with each other (Fig. S1b); at 3 h, the samples were obviously composed of the cross-connected rods combining side-by-side (Fig. S1c); at 4 h, the small size nanorods further became bigger, with ca. 1 μm in length and ca. 100-200 nm in width (Fig. S1d); at 5 h, the bigger rods started to combine side by side again and turned into a big-size rod, which was more than 1 μm length and 200 nm width (Fig. S1e). After the reaction time was increased up to 24 h, the 1D nanorods of several micrometers length were finally formed with the prolonged reaction time (Fig. S1f-h).

With the above observations, the attachment-recrystallization growth mechanism for the formation of Bi_2S_3 nanorods is proposed. The growth process of Bi_2S_3 nanorods indicates that their growth involved four main processes (Scheme S1): (1) the formation of thin and short nanorods from primary nanoparticles, which was a crucial step in the successful formation of the final nanorods; (2) the thin and short nanorods served as building blocks attached together side-by-side, because small nanocrystals had high surface energy and prone to congregate with each other; (3) the side-by-side attached nanorods grow into long and wide nanorods *via* Ostwald ripening process; and (4) repeating the processes of (2) and (3) to further reduce the surface energy by recrystallization.

Table S1 Chemical composition of the as-prepared Pd_4S/Bi_2S_3 hybrid (PdBi-1)

Element	Weight %	Atom %
S K	20.40	60.06
Pd L	9.14	8.11
Bi M	70.47	31.83
Total	100.01	100.00

Table S2 The reaction rate constants on the different catalysts

Sample	Pseudo-first-order rate constant ($\times 10^{-3}$ min^{-1})	Regression square (R^2)
Bi_2S_3	4.56	0.9892
PdBi-1	11.21	0.9307
PdBi-3	6.1	0.9993
PdBi-2	4.78	0.9115
BiPd sp	2.94	0.9704
P25	1.88	0.9968
Photo	1.08	0.9791

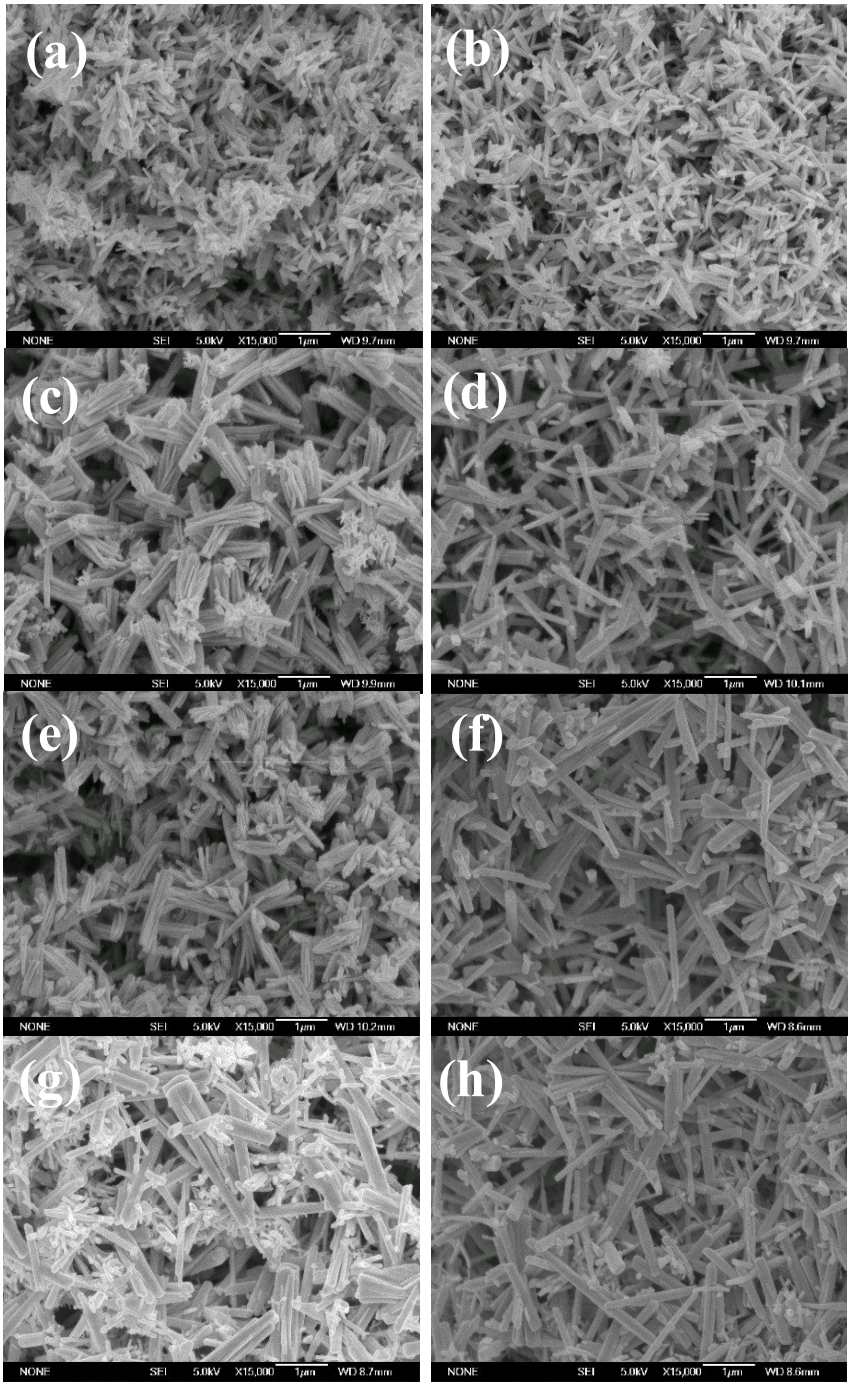

Fig. S1 SEM images of the Bi_2S_3 nanostuctures at different reaction times: (a) 1 h, (b) 2 h, (c) 3 h, (d) 4 h, (e) 5 h, (f) 10 h, (g) 16 h, and (h) 24 h.

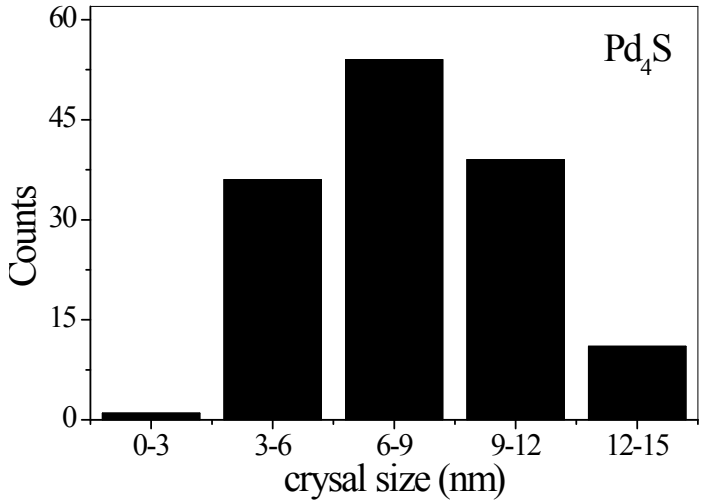

Fig. S2 Particle size distribution of Bi_2S_3 in the Pd_4S/Bi_2S_3 hybrid (PdBi-1).

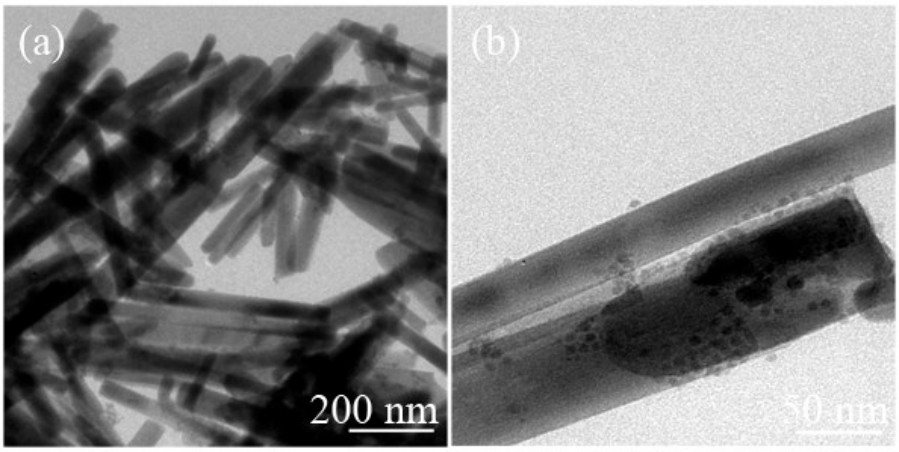

Fig. S3 (a) Low- and (b) high-magnified TEM images of the Pd_4S/Bi_2S_3 hybrid (PdBi-2, staring ratio).

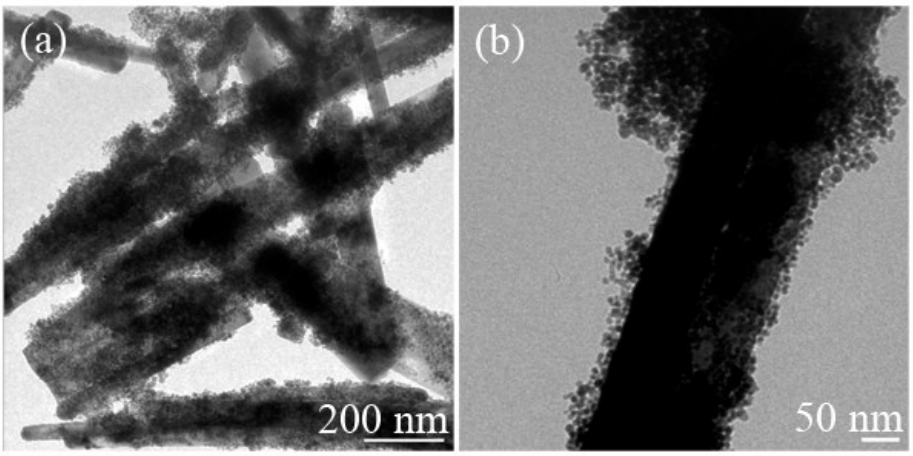

Fig. S4 (a) Low- and (b) high-magnified TEM images of the Pd_4S/Bi_2S_3 hybrid (PdBi-3, staring ratio).

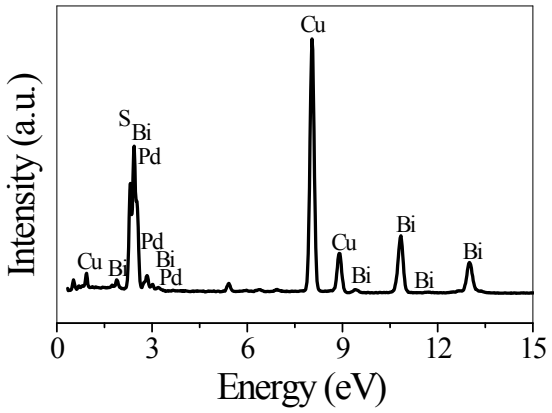

Fig. S5 EDS spectrum of the Pd_4S/Bi_2S_3 hybrid (PdBi-1, staring ratio).

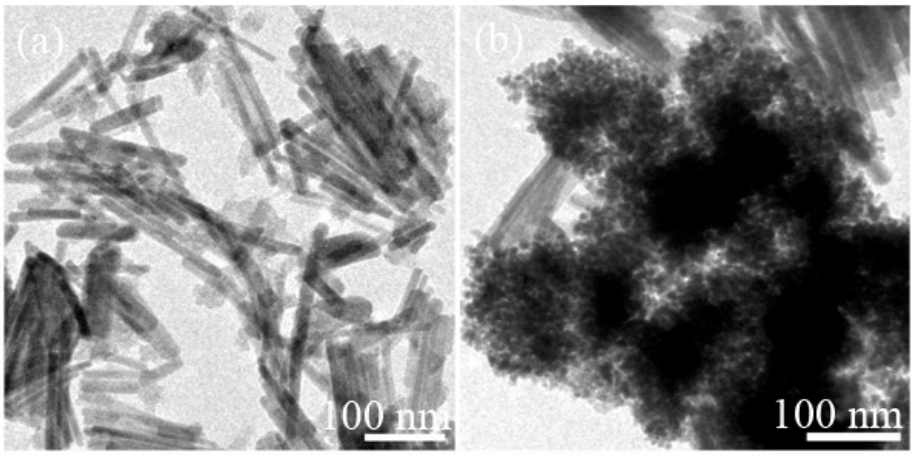

Fig. S6 TEM images of (a) the Bi_2S_3 nanorods and (b) the Pd_4S/Bi_2S_3 hybrids (reaction for 10 min).

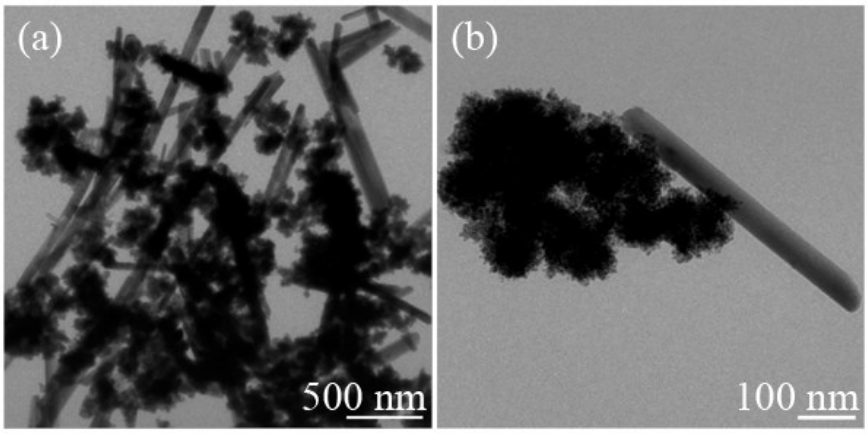

Fig. S7 TEM images of the Pd_4S nanoparticles separated from the Bi_2S_3 nanorods (PdBi sp).

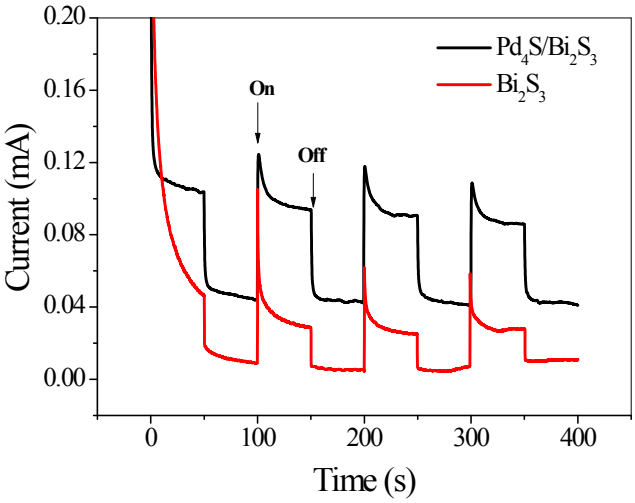

Fig. S8 Current-time curves of the Bi_2S_3 nanorods and Pd_4S/Bi_2S_3 hybrid (PdBi-1) at a bias of 0.25 V under chopped visible light illumination ($\lambda > 420$ nm).

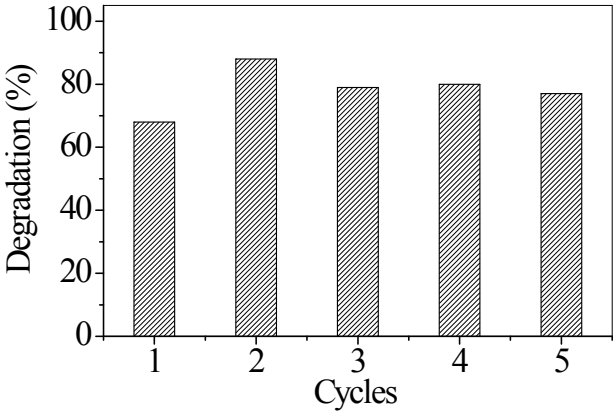

Fig. S9 Cycling degradation of Atrizine on the Pd_4S/Bi_2S_3 hybrid (PdBi-1).

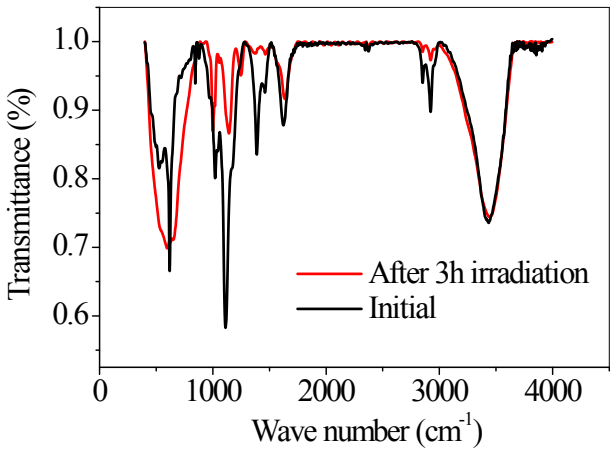

Fig. S10 FTIR spectra of the as-prepared Pd_4S/Bi_2S_3 hybrid: initial (blank) and after 3-h irradiation (red). After 3-h irradiation, the absorption peaks of some functional groups, such as -CH_2-CH_2-(1381cm^{-1}, 1470 cm^{-1}, 2931 cm^{-1}), C=C(1650 cm^{-1}) and -C-O-C-(1137cm^{-1}), decreased.

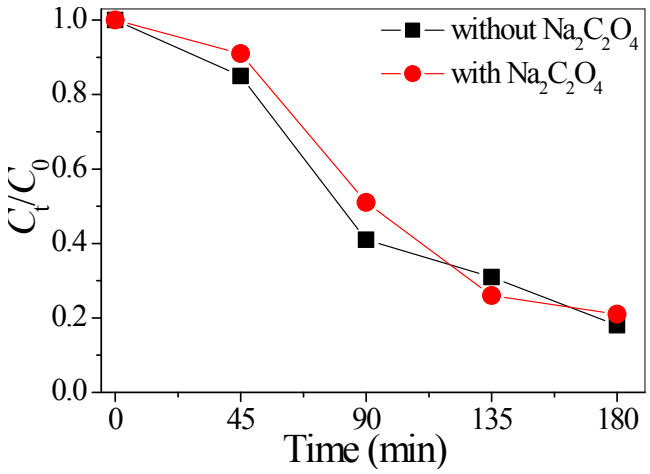

Fig. S11 Hole-capturing testing results of the Pd_4S/Bi_2S_3 hybrid for the photocatalytic degradation of Atrazine under visible light irradiation.

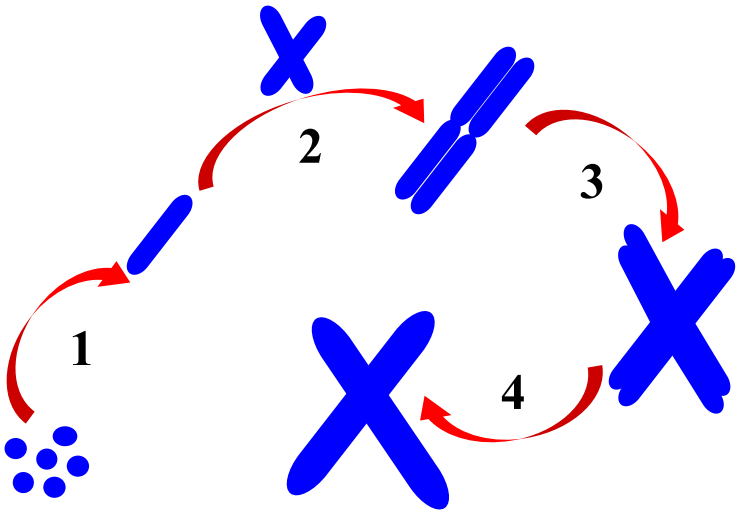

Scheme S1 The proposed Bi_2S_3 nanorods formation mechanism.

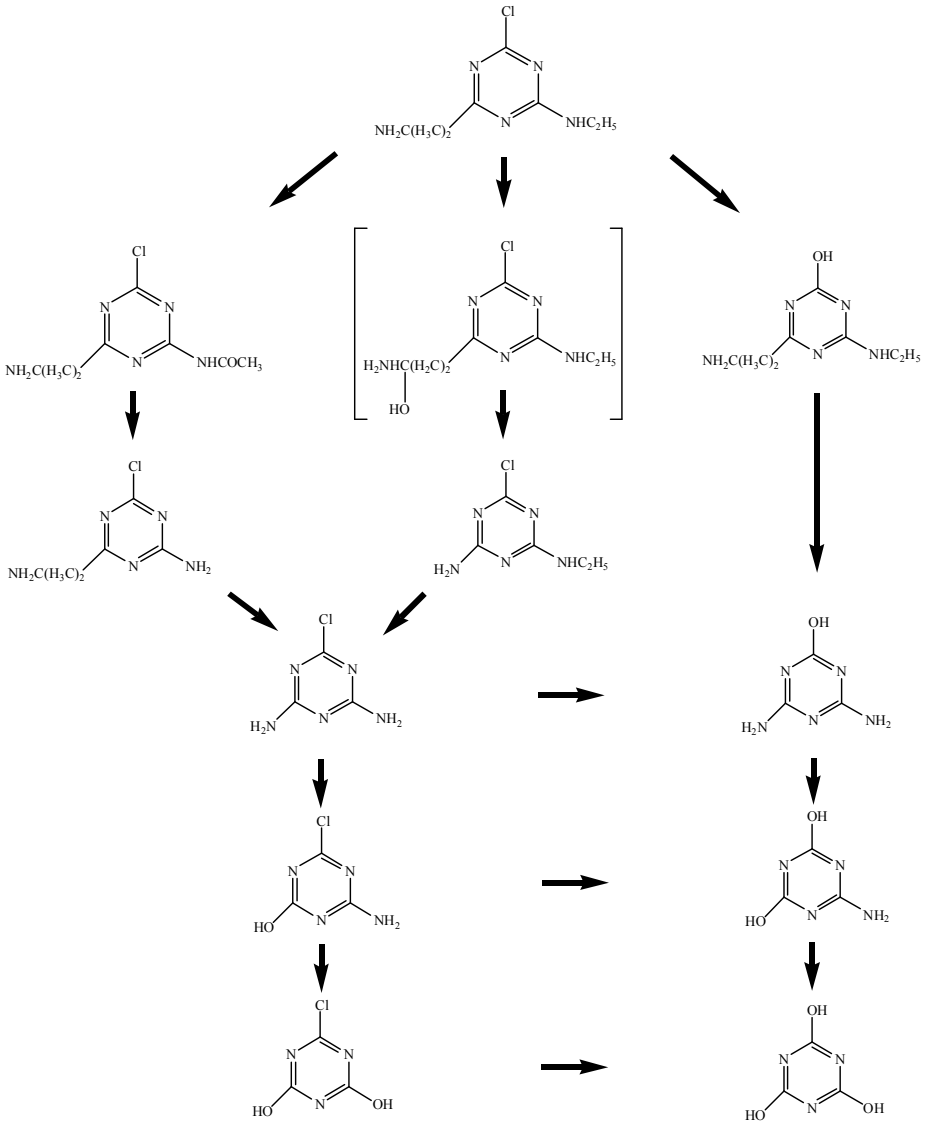

Scheme S2 The proposed photocatalytic Atrazine degradation pathway on the Pd_4S/Bi_2S_3 hybrid.